A Laser Obstacle Avoidance System for Manned and Unmanned Aircraft Detect-and-Avoid

Conference Paper · February 2015

DOI: 10.13140/2.1.1275.7285

CITATIONS
9

READS
497

3 authors:

Subramanian Ramasamy
RMIT University
122 PUBLICATIONS **1,431** CITATIONS
SEE PROFILE

Alessandro Gardi
RMIT University
139 PUBLICATIONS **1,394** CITATIONS
SEE PROFILE

Roberto Sabatini
RMIT University
394 PUBLICATIONS **2,997** CITATIONS
SEE PROFILE

A Laser Obstacle Avoidance System for Manned and Unmanned Aircraft Detect-and-Avoid

Subramanian Ramasamy, Alessandro Gardi and Roberto Sabatini
School of Aerospace, Mechanical and Manufacturing Engineering, RMIT University
Melbourne, VIC 3000, Australia

Abstract

This paper reviews the main hardware/software characteristics and the numerical simulations performed to validate the functionalities of an obstacle warning and avoidance system for various manned and unmanned platform applications. The Laser Obstacle Avoidance and Monitoring (LOAM) system is one of the key non-cooperative sensors adopted for avoiding obstacles/intruders. Robust multi-criteria decision logics are adopted to identify the optimal avoidance manoeuvre considering all currently and previously detected obstacles by employing a so-called history function. Additionally, a new formulation is adopted for defining the overall uncertainty volumes associated with the detected obstacles. The demonstrated detection performances and the robust trajectory generation algorithm ensure a safe avoidance of all classes of obstacles (i.e. ground and aerial) in most weather conditions and flight phases.

Keywords: Airborne Lasers, Detect-and-Avoid, Integrated Systems, Aerospace Electronics Systems, Laser Performance, Eye-Safety, Laser Test and Evaluation.

Introduction

The widespread adoption of small-to-medium size Remotely Piloted Aircraft Systems (RPAS) in low-level or nap-of-the-earth flight missions has resulted in growing public concerns regarding the overall safety of people and property. In this context, obstacle detection, warning and avoidance capabilities are of paramount importance to ensure the safety of flight operations. The Laser Obstacle Avoidance and Monitoring (LOAM) system was originally developed and tested on rotary-wing platforms [1-4], and the development of a scaled version for small-to-medium size RPAS is currently being performed [5-7]. The LOAM detects potentially dangerous obstacles placed in or nearby the nominal RPAS flight trajectory, classifies and stores the detected obstacles, and provides guidance for optimal avoidance manoeuvres, as well as timely caution/warnings to the ground crew (both aural and visual).

Hardware Architecture

The main components of the LOAM are the Sensor Head Unit (SHU), the Processing Unit (PU), the Control Panel (CP) and the Display Unit (DU). An exploded view of the SHU of the original LOAM version for rotorcraft is depicted in Fig. 1. The laser beam originating in the LOAM SHU is electro-mechanically orientated to periodically scan the area around the nominal flight trajectory inside a Field of View (FOV) of 40° in azimuth and 30° in elevation, with an adjustable Field of Regard (FOR) capability of ± 20° on azimuth, centred on the longitudinal axis of the platform. The resulting laser scanning pattern is represented in Fig. 2. The LOAM integrated architecture is illustrated in Fig. 3. The PU, in particular, interacts with the RPAS Mission Management System (MMS) [8-10], which is integrated with the

multisensory navigation system [11, 12] and the Detect-and-Avoid (DAA) system [13-15]. RPAS command and telemetry data-links serve as the communication media between the platform and the ground systems. The CP and DU are adopted based on the specific unmanned platform employed.

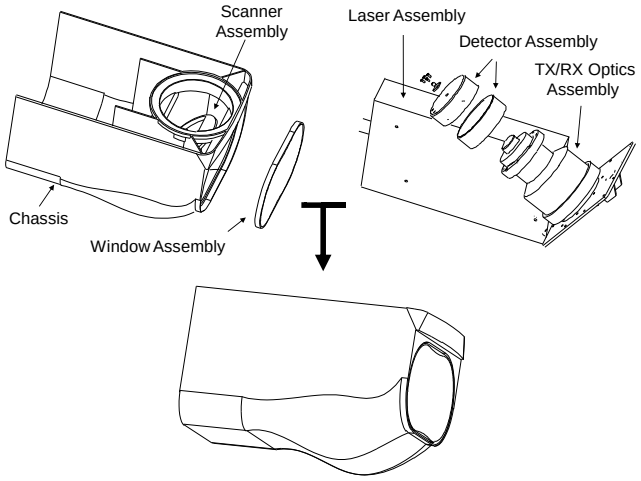

Fig.1: Exploded and assembly views of the LOAM SHU. Adapted from [4].

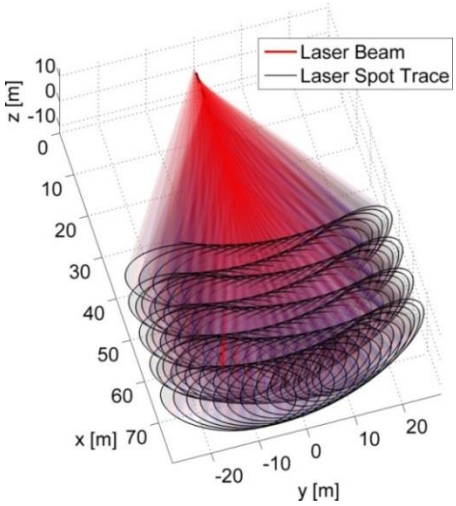

Fig. 2: Scanning pattern of the LOAM laser beam.

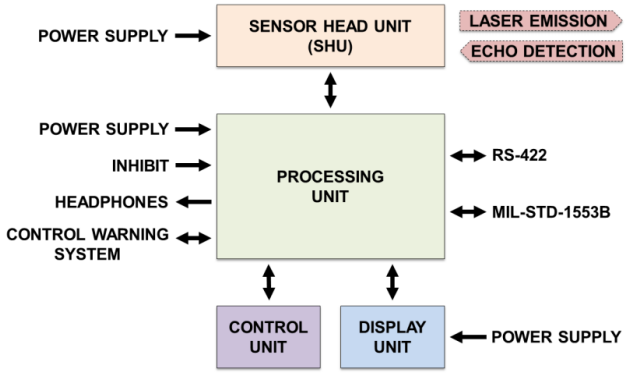

Fig. 3: LOAM hardware architecture showing the interfaces for avionics integration [7].

Architecture

The signal processing software architecture is represented in Fig. 4. The LOAM performs echo detection through analogue signal processing that consists of an optical-electrical conversion, a signal pre-amplification and a threshold comparison. Dedicated digital processing algorithms subsequently determine the obstacle positions and characteristics independently from the platform motion. Ground obstacles including wires, poles and extended structures and aerial obstacles are detected by the LOAM system. The shapes of all detected obstacles are reconstructed without using additional navigation data in slow-moving platforms. In platforms with high dynamics capabilities, the data from LOAM are integrated with the navigation sensor data as part of an integrated navigation and guidance system. Reliable detection is performed by local analysis on single echoes and thus the range, angular coordinates and other features of the obstacle are obtained. Successively, global analysis is performed in order to group the echoes detected during a scan period and to reconstruct the shape of the obstacles.

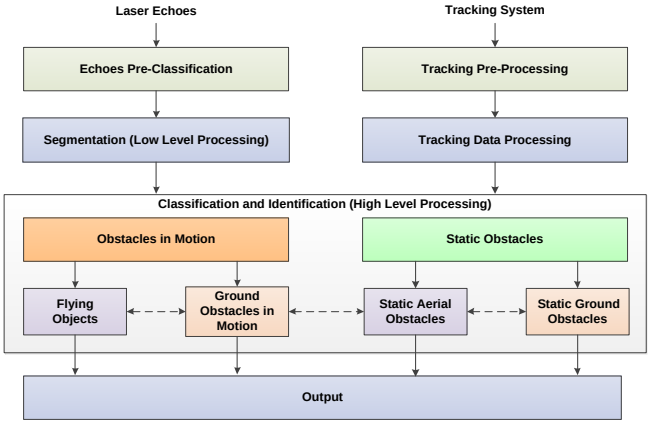

Fig. 4: LOAM signal processing software architecture.

One of the main challenges in the integration of RPAS into non-segregated airspace is the DAA capability that enables the unmanned platforms to perform equally or exceed the performance of the see-and-avoid ability of the pilot in manned aircraft systems. Both cooperative and non-cooperative DAA systems are being developed to enable RPAS to routinely access all classes of airspace In order to provide automated avoidance functionalities, the LOAM employs three key algorithms namely; prediction of the future platform trajectory, calculation of the potential collisions with the detected obstacles and generation of a set of optimal avoidance trajectories in case a risk of collision is determined. Identification and evaluation of the required sensors, as well as the associated data fusion algorithms, are a key constituent of the DAA system design. A number of cooperative systems and non-cooperative sensors can be employed in the DAA system design. The inclusion of ADS-B redefines the paradigm of Communication, Navigation and Surveillance (CNS) in Air Traffic Management (ATM) today by providing trajectory information. The non-cooperative DAA sensors are employed to detect intruders or other obstacles in the RPAS Field of Regard (FOR) when cooperative systems are unavailable in the intruders. Optical, thermal, LIDAR, Millimetre Wave (MMW) Radar and acoustic sensors are employed part of non-cooperative DAA system. The DAA technologies are listed in Table 1 representing C for cooperative and NC for non-cooperative (both active and passive) sensors [13]. Based on the identified technologies, Boolean logic based decision tree architecture for the DAA system is illustrated in Fig. 5.

Table 1: DAA candidate technologies

Sensor/ System	Type	Range	Bearing	Trajectory
Visual camera	NC, Passive	-	Accurate	Extracted
Thermal camera	NC, Passive	-	Accurate	Extracted
LOAM	NC, Active	Accurate	Narrow	Extracted
MMW Radar	NC, Active	Accurate	Narrow	Extracted
Acoustic	NC, Active	Accurate	360º	Extracted
ADS-B	C	Accurate	Calculated	Provided
TCAS/ ACAS	C	Accurate	Accurate	Extracted

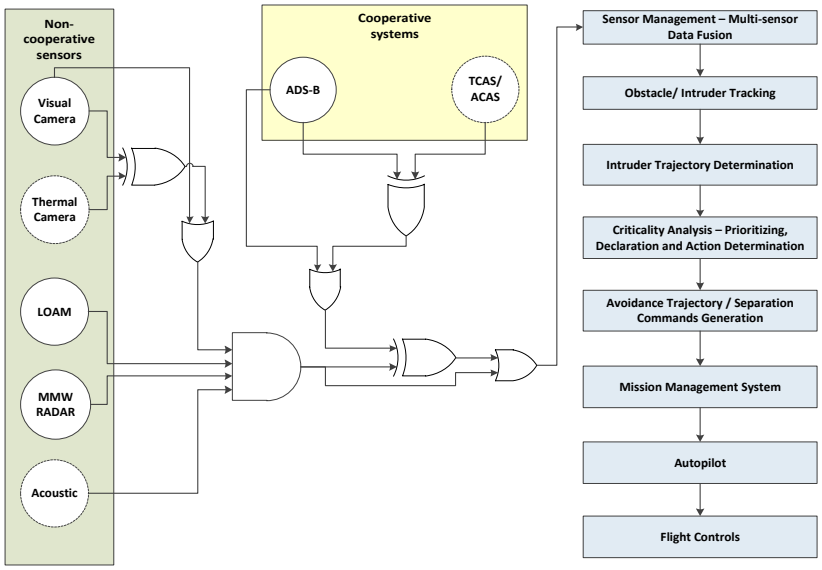

Fig. 5: DAA system architecture.

The sequential steps involved in the DAA process for executing an efficient Track, Decide and Avoid (TDA) loop are illustrated in Fig. 5. The trajectory information of the intruders is determined after performing multi-sensor data fusion. Criticality analysis is carried out to prioritize (i.e. to determine if a collision risk threshold is exceeded for all tracked intruders) and to determine the action commands. If an avoidance action is required, the DAA system generates and optimises an avoidance trajectory according to a priority based cost function based on minimum distance, fuel, time and closure rate criteria with the aid of differential geometry algorithms [10] to generate a smooth trajectory. Current research is also addressing virtual obstacle detection and avoidance including GNSS unintentional and intentional radiofrequency signal interference (i.e., jamming and spoofing), no-fly zones, noise-sensitive areas and wake turbulence regions.

Avoidance Trajectory Generation

The original avoidance trajectories generation algorithm for rotorcraft platforms was introduced in [4]. The algorithms for the generation of the avoidance trajectories in fixed-wing platforms were presented in [7]. Similarly to the rotorcraft case, the algorithm for fixed-wing aircraft follows the dynamic programming approach. A direct optimisation method is implemented therefore the algorithm is based on the aircraft dynamics, and not on a geometric trajectory model. Robust decision logic is subsequently introduced to select the trajectory to be flied based on multiple criteria. The approximated dynamic model of the fixed-wing platform is based on a point-mass rigid body with three linear degrees of freedom (3-DoF) with constant mass. During the entire approach to the obstacle, the vehicle control system can provide a linear variation of μ, up to the assumed maximum bank angle. This can be expressed as:

$$\begin{cases} \mu = \mu_0 + \dot{\mu}_{MAX} \cdot t & (\mu \leq \mu_{MAX}) \\ \dot{\mu} = 0 & (\mu = \mu_{MAX}) \end{cases} \quad (1)$$

The maximum roll rate was set at $\dot{\mu}_{MAX} = 20\,°/s$. The algorithms for estimation of the obstacle absolute motion based on differential geometry approach were introduced in [15]. In order to provide the fast and reliable performance required for our safety-critical task, the

avoidance trajectory generation is based on simplified geometric shapes. The standard deviation of the LOAM detection and tracking error for each axis is given by:

$$\sigma_{(X,Y,Z)} = \sqrt{\sigma^2_{\text{range}_{(x,y,z)}} + \sigma^2_{\text{azimuth}_{(x,y,z)}} + \sigma^2_{\text{elevation}_{(x,y,z)}}} \quad (2)$$

In particular, given the different values of uncertainty associated with the three cardinal directions, an ellipsoidal avoidance volume is implemented in the algorithm. In order to assure adequate safety levels, a separation buffer is introduced, which inflates the ellipsoidal avoidance volume associated with the obstacle. In particular, to provide a confidence level of 95%, the uncertainty associated with the position of an obstacle is calculated as twice the standard deviation (i.e. the two-sigma) of the total obstacle detection and tracking errors. When the distance between two detected obstacles is comparable with the calculated uncertainty values, or with the RPAS dimensions, the algorithm combines the two obstacles in a single avoidance volume. The subsequent step involves the selection of the optimal trajectory from the generated set of safe trajectories, which is then fed to the aircraft guidance subsystems. The implemented decision logic is based on minimisation of the following cost function:

$$J = w_t \cdot t_{SAFE} + w_f \int [SFC \cdot T(t)]dt - w_d \int D(t)dt \quad (3)$$

where t_{SAFE} is the time at the point of minimum distance from the detected obstacles, hence it corresponds to the attainment of a safe condition, $SFC\,[\frac{kg}{N} \cdot s]$ is the specific fuel consumption, $T(t)$ is the thrust profile, $D(t)$ is the distance from the ellipsoidal avoidance volume of the obstacle and w_t, w_f, w_d are the weightings attributed to time, fuel and integral distance respectively. In time-critical avoidance applications (i.e., closing-up obstacles with high relative velocities and/or accelerations) appropriate higher weightings are used for the time and distance cost elements.

Uncertainty analysis

Error analysis is performed to determine the overall uncertainty volume in the airspace surrounding the intruder track based on SAA Unified Method (SUM). This is accomplished by considering both the navigation and the tracking errors affecting the measurements and translating them to unified range and bearing uncertainty descriptors. In order to quantify the errors, let σ_{Ex}, σ_{Ey} and σ_{Ez} represent the standard deviation of the navigation error (σ_{nx}, σ_{ny}, σ_{nz}) or the tracking error (σ_{tx}, σ_{ty}, σ_{tz}) in the x, y and z directions respectively. The ellipsoid is assumed to be located at the origin. Using a spherical coordinates frame with origin at the host RPAS centre of mass, the range and bearing errors associated with the intruder tracking process are transformed into a local Cartesian coordinate frame (either host or intruder body frame). The transformation process results in the generation of navigation and tracking error ellipsoids defined as [26]:

$$\frac{x^2}{{\sigma_{Ex}}^2} + \frac{y^2}{{\sigma_{Ey}}^2} + \frac{z^2}{{\sigma_{Ez}}^2} = 1 \quad (4)$$

(R, θ, φ) are the spherical coordinates defined on a point P. The Cartesian coordinates of the surface points are given by:

$$x_{ij} = R\sin(\theta_i)\cos(\varphi_j) \quad (5)$$

$$y_{ij} = R\sin(\theta_i)\sin(\varphi_j) \quad (6)$$

$$z_{ij} = R\cos(\theta_i) \quad (7)$$

In order to develop a generalized solution towards obtaining a unified approach to cooperative and non-cooperative DAA, the ellipsoids are subjected to two transforms: rotation, R and translation, T (projection along LOS). The inverse transform of one ellipsoid with respect to another, L can be expressed as:

$$L^{-1} = R^{-1}\, T^{-1} L \tag{8}$$

The coordinates of the centre, P should satisfy the condition:

$$\frac{x^2}{(\sigma_{nx} \pm \sigma_{tx})^2} + \frac{y^2}{(\sigma_{ny} \pm \sigma_{ty})^2} + \frac{z^2}{(\sigma_{nz} \pm \sigma_{tz})^2} = 1 \tag{9}$$

The simplification of the above equation results considering multivariate Gaussian statistics results in a quadratic condition that is used to derive the miss, tangential and intersection conditions based on the resultant discriminant. Vector analysis is applied to the navigation and tracking ellipsoids. Let $\vec{X}$ denote the points on the surface of the ellipsoid. The components of $\vec{X}$ are X_1 = x, X_2 = y and X_3 = z. Let the surface normal vector be denoted as $\hat{n}$. The normal vector can be expressed as :

$$\hat{n} = \frac{\overrightarrow{X_\theta} \times \overrightarrow{X_\varphi}}{\left|\overrightarrow{X_\theta} \times \overrightarrow{X_\varphi}\right|} \tag{10}$$

The differential surface area element, $d\Lambda$ which is an area of a patch of the surface at $r(\theta, \varphi)$ is given by :

$$d\Lambda = S\, d\theta\, d\varphi \tag{11}$$

$$S = \left|\overrightarrow{X_\theta} \times \overrightarrow{X_\varphi}\right| \tag{12}$$

The decomposition can be expressed in terms of parameters A, B and C given by :

$$A = \overrightarrow{X_\theta} . \overrightarrow{X_\theta} \tag{13}$$

$$B = \overrightarrow{X_\theta} . \overrightarrow{X_\varphi} \tag{14}$$

$$C = \overrightarrow{X_\varphi} . \overrightarrow{X_\theta} \tag{15}$$

The parameters D, E and F are given by :

$$D = -\overrightarrow{X_\theta} . \hat{n}_\theta \tag{16}$$

$$E = \frac{1}{2} \left(\overrightarrow{X_\theta} . \hat{n}_\varphi + \overrightarrow{X_\varphi} . \hat{n}_\theta\right) \tag{17}$$

$$F = -\overrightarrow{X_\varphi} . \hat{n}_\varphi \tag{18}$$

The derivatives of the decomposition of the above parameters can be expressed as:

$$\frac{\delta r(\theta,\varphi)}{\delta\theta} = r_\theta \tag{19}$$

$$\frac{\delta^2 r(\theta,\varphi)}{\delta\theta^2} = r_{\theta\theta} \tag{20}$$

and other derivatives. The parameters D, E and F involve vector products of the derivatives of the components of $\vec{X}$ and $\hat{n}$. The parameter S is expressed in spherical harmonics as:

$$S = r\left[{r_\varphi}^2 + {r_\theta}^2 (\sin\theta)^2 + r^2 (\sin\theta)^2\right]^{1/2} \tag{21}$$

The shape of the combined navigation and tracking uncertainty volume (accounting for both uncorrelated or correlated sensor measurements) is conveniently described using spherical

harmonics. Let $r(\theta,\psi)$ represent the smooth function defined on the ellipsoid and the parameterization of this spherical harmonic representation is given by:

$$r(\theta,\varphi) = \sum_{l=0}^{\infty} \sum_{m=-l}^{l} X_{lm}\, Y_{lm}(\theta,\varphi) \tag{22}$$

The function $r(\theta,\psi)$ is limited to a number of N finite coefficients and l and m represent the direction index. X_{lm} is a factor and the function $Y_{lm}(\theta,\psi)$ is the spherical harmonic function and is given by:

$$Y_{lm}(\theta,\psi) = \sqrt{\frac{(2l+1)(l-m)!}{4\pi(l+m)!}}\, P_{lm}\cos(\theta)\, e^{im\psi} \tag{23}$$

where P_{lm} represents the Legendre functions. The Legendre polynomial function is given by:

$$P_{lm}(x) = \frac{1}{2^n n!}\frac{d^n(x^2-1)^n}{dx^n} \tag{24}$$

Expanding $e^{im\psi}$ as $C_{lm}\cos(m\psi) + i\, S_{lm}\cos(m\psi)$, we have C_{lm} and S_{lm} defined as the spherical harmonic coefficients. The spherical harmonic coefficients are obtained as [27]:

$$L_{lm} = \{C_{m0},\ S_{lm} \text{and } C_{lm}\} \tag{25}$$

$$S_{lm} = 0;\ \ l, m\ \varepsilon\ N \tag{26}$$

$$C_{lm} = 0;\ \ l, m\ \varepsilon\ 2N+1 \tag{27}$$

and for all other l, m:

$$C_{lm} = \frac{3}{a^l}\frac{\left(\frac{l}{2}\right)!\left(\frac{l}{m}\right)!(2-\delta_{om})}{2^m(l+3)(l+1)!} \times \sum_{i=0}^{(l-m)/4}\frac{(a^2-b^2)^{(m+4i)/2}[c^2-\left(\frac{1}{2}\right)(a^2-b^2)]^{(l-m-4i)/2}}{16^i\left(\frac{l-m-4i}{2}\right)!\left(m+\frac{2i}{2}\right)!i!} \tag{28}$$

where δ_{om} is the Kronecker symbol and (a, b, c) represents the semi-major radius of the navigation or tracking error ellipsoid. C_{m0} are the zonal coefficients (functions of latitude) while S_{lm} and C_{lm} are the tesseral coefficients (functions of longitudes). When l=m, sectorial coefficients are obtained which are functions of both latitudes and longitudes. Finally, the overall uncertainty volume is obtained by combining the two error ellipsoids. When the errors are correlated tensors analysis is adopted to properly account for covariant or contravariant components. Six components are associated with a rank-2 symmetrical tensor ϕ_{ij}, which are three diagonal and three off-diagonal components usually occurring in pairs. The ellipsoid associated with the tensor is given by:

$$r_i \phi_{ij} r_j = 1 \tag{29}$$

where r is the radius vector having components r_i and r_j. Considering a three-dimensional space, the covariance tensor for the error ellipsoid is given as:

$$T = \begin{bmatrix} \phi_{ii} & \phi_{ij} & 0 \\ \phi_{ji} & \phi_{jj} & 0 \\ 0 & 0 & \phi_{kk} \end{bmatrix} \tag{30}$$

for components (i, j, k) along (X, Y, Z) axes. The partial derivatives of an invariant function provide the components of a covariant vector. A contravariant vector is the same as a contravariant tensor of first order.

Simulation and Results

Simulation activities were performed to validate the avoidance trajectory generation algorithm and to assess its performance. A realistic three-dimensional scenario for obstacle

avoidance was introduced. The RPAS equipped with the LOAM is flying at an altitude z = 100 m Above Ground Level (AGL) and approaching a number of obstacles. The original horizontal flight trajectory would lead to a collision with the obstacle. After a successful detection of all the wires, the algorithm calculates the distances among each of them. A representative set of avoidance trajectories generated following these assumptions, is depicted in Fig. 6. Fig. 7 illustrates the separation envelopes between the RPAS and the boundary surface of the ellipsoidal avoidance volumes obtained from the uncertainty analysis described before, calculated for each point of the calculated trajectories.

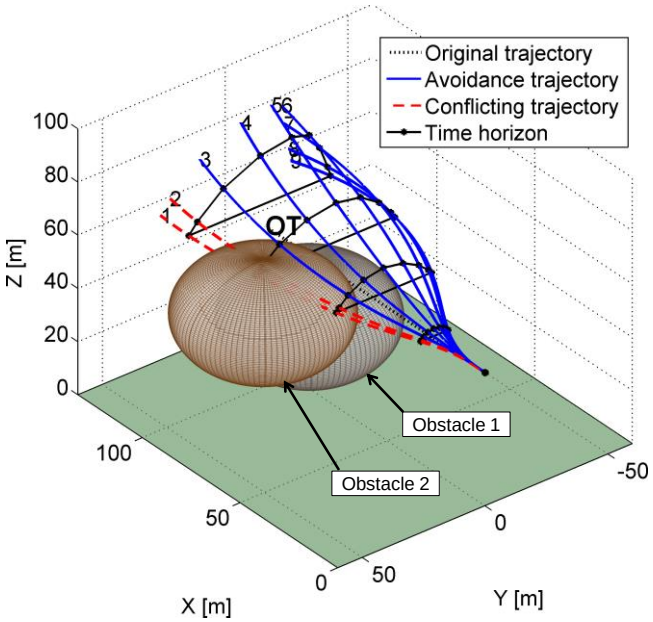

Fig. 6: Results of the avoidance trajectory generation algorithm.

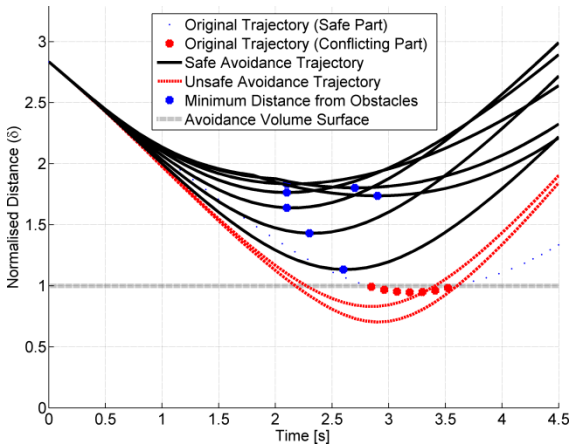

Fig. 7: Absolute distance of the trajectories from ellipsoidal avoidance volume boundaries.

Human Machine Interface and Interaction

Dedicated LOAM CP and DU are being developed for RPAS applications. Their characteristics are conceptually similar to the ones developed for the manned aircraft versions. However, as these CP and DU are integrated in the Remote Piloting Station (RPS) and will be operated by the remote pilot, in this case the LOAM operating modes are activated using two different communication data links for Line-of-Sight (LOS) and Beyond

LOS (BLOS) operations. Fig. 8 shows some synthetic display formats currently being developed for the RPAS version. In particular, Fig. 8a depicts the safety line, which connects the points of minimum pitch for safe obstacle avoidance at all azimuths. Fig 8b depicts the synthetic vision format integrating information from the LOAM and from Forward Looking Sensor (FLS) systems.

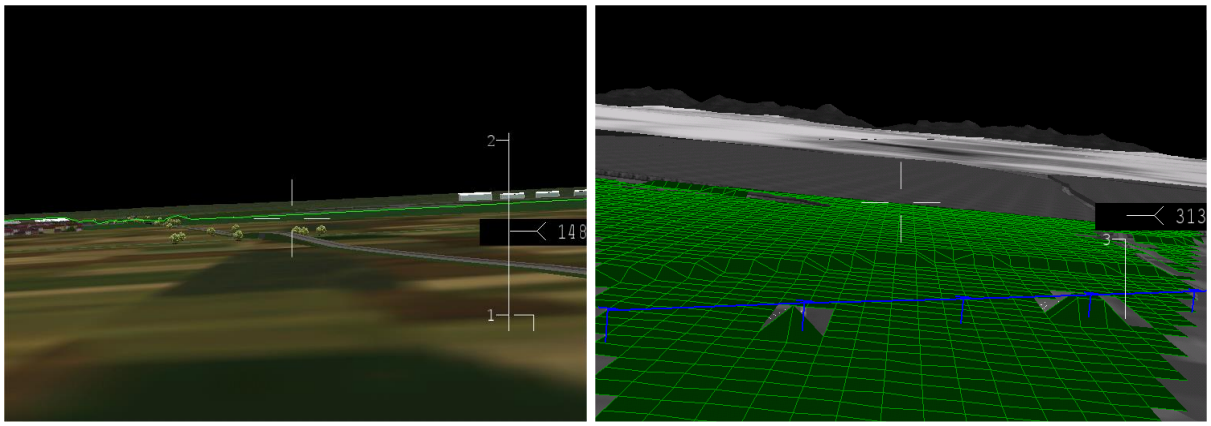

(a) *(b)*

Fig. 8: Synthetic display formats developed for the Remote Piloting Station (RPS) of RPAS.

Conclusion

This paper briefly reviewed the hardware and software design of the Laser Obstacle Avoidance and Monitoring (LOAM) system, which was originally designed for rotorcraft and is currently being developed for small-to-medium size Remotely Piloted Aircraft Systems (RPAS). The LOAM system is employed as one of the non-cooperative sensors in an integrated Detect-and-Avoid (DAA) architecture. The algorithms for avoidance trajectory generation/optimisation, uncertainty analysis for determination of the overall avoidance volume and simulation results have been presented. Current research activities are addressing the integration of LOAM with Forward Looking Sensors (FLS) and Night Vision Imaging Systems (NVIS) [19]. Display formats currently being developed for the RPAS remote pilot station include a Safety Line (SL) format, a Wires & Poles (WP) format, an All Obstacles (AO) format and an Integrated LOAM/FLS (ILF) format. Additional mathematical descriptors including covariant and contravariant tensors are being adopted for uncertainty volume determination, toward a unified analytical approach covering both cooperative and non-cooperative Detect-and-Avoid (DAA) applications. The possible integration of LIDAR with other RPAS avionic sensors is being studied and future research will address the DAA functionalities required for 4-Dimensional Trajectory Based Operations (4D-TBO) [9, 10, 20, 21].

References

1. Sabatini, R., "Tactical Laser Systems Performance Analysis in Various Weather Conditions", in RTO-MP-001 - E-O Propagation, Signature and System Performance under Adverse Meteorological Conditions Considering Out of Area Operations, pp. 29-1 to 29-13, NATO Research and Technology Organization (RTO), Naples, Italy, 1998.
2. Sabatini, R., Guercio, F., and Vignola, S., "Airborne laser systems performance analysis and mission planning", in RTO-MP-046 - Advanced Mission Management and Systems

Integration Technologies for Improved Tactical Operations, NATO Research and Technology Organization (RTO), Florence, Italy, 1999.

3. Sabatini, R., Roviaro, E., and Cottalasso, M., "Development of a Laser Collision Avoidance System for Helicopters: Obstacle Detection/Classification and Calculation of Alternative Flight Paths", in RTO-MP-092 - Complementarity of Ladar and Radar, NATO Research and Technology Organization (RTO), 2002.
4. Sabatini, R. and Richardson, M. A., Airborne Laser Systems Testing and Analysis: NATO Science and Technology Organization, 2010.
5. Sabatini, R., Gardi, A., and Ramasamy, S., "A Laser Obstacle Warning and Avoidance System for Unmanned Aircraft Sense-and-Avoid", Applied Mechanics and Materials, vol. 629, pp. 355-360, 2014. DOI: 10.4028/www.scientific.net/AMM.629.355
6. Sabatini, R., Gardi, A., Ramasamy, S., and Richardson, M. A., "A Laser Obstacle Warning and Avoidance System for Manned and Unmanned Aircraft", in proceedings of IEEE Metrology for Aerospace (MetroAeroSpace 2014), Benevento, Italy, 2014, pp. 616-621. DOI: 10.1109/MetroAeroSpace.2014.6865998
7. Sabatini, R., Gardi, A., and Richardson, M. A., "LIDAR Obstacle Warning and Avoidance System for Unmanned Aircraft", International Journal of Mechanical, Aerospace, Industrial and Mechatronics Engineering, vol. 8, pp. 62-73, 2014.
8. Ramasamy, S., Sabatini, R., and Gardi, A., "Unmanned Aircraft Mission Management System for Trajectory Based Operations", in proceedings of 4th Australasian Conference on Unmanned Systems (ACUS 2014), Melbourne, Australia, 2014. DOI: 10.13140/2.1.1695.6488
9. Ramasamy, S., Sabatini, R., Gardi, A., and Kistan, T., "Next Generation Flight Management System for Real-Time Trajectory Based Operations", Applied Mechanics and Materials, vol. 629, pp. 344-349, 2014. DOI: 10.4028/www.scientific.net/AMM.629.344
10. Ramasamy, S., Sabatini, R., Gardi, A., and Liu, Y., "Novel flight management system for real-time 4-dimensional trajectory based operations", in proceedings of AIAA Guidance, Navigation, and Control Conference 2013 (GNC 2013), Boston, MA, USA, 2013. DOI: 10.2514/6.2013-4763
11. Sabatini, R., Bartel, C., Kaharkar, A., Shaid, T., and Ramasamy, S., "Navigation and Guidance System Architectures for Small Unmanned Aircraft Applications", International Journal of Mechanical, Aerospace, Industrial and Mechatronics Engineering, vol. 8, pp. 733-752, 2014
12. Sabatini, R., Ramasamy, S., Gardi, A., and Rodriguez Salazar, L., "Low-cost sensors data fusion for small size unmanned aerial vehicles navigation and guidance", International Journal of Unmanned Systems Engineering, vol. 1, pp. 16-47, 2013. DOI: 10.14323/ijuseng.2013.11
13. Ramasamy, S., Sabatini, R., and Gardi, A., "Towards a Unified Approach to Cooperative and Non-Cooperative RPAS Detect-and-Avoid", in proceedings of 4th Australasian Conference on Unmanned Systems (ACUS 2014), Melbourne, Australia, 2014. DOI: 10.13140/2.1.4841.3764
14. Ramasamy, S., Sabatini, R., and Gardi, A., "Avionics Sensor Fusion for Small Size Unmanned Aircraft Sense-and-Avoid", in proceedings of IEEE Metrology for Aerospace (MetroAeroSpace 2014), Benevento, Italy, 2014. DOI: 10.1109/MetroAeroSpace.2014.6865933

15. Rodriguez Salazar, L., Sabatini, R., Gardi, A., and Ramasamy, S., "A Novel System for Non-Cooperative UAV Sense-and-Avoid", in proceedings of European Navigation Conference 2013 (ENC 2013), Vienna, Austria, 2013.
16. Sabatini, R. and Richardson, M. A., "Airborne Laser Systems Testing, Safety Analysis, Modelling and Simulation", presented at the 21st Annual Symposium of the Society of Flight Test Engineers - European Chapter, Vergiate (VA), Italy, 2010.
17. Sabatini, R. and Richardson, M. A., "Novel atmospheric extinction measurement techniques for aerospace laser system applications", Infrared Physics and Technology, vol. 56, pp. 30-50, 2013. DOI: 10.1016/j.infrared.2012.10.002
18. Sabatini, R., Richardson, M. A., Jia, H., and Zammit-Mangion, D., "Airborne laser systems for atmospheric sounding in the near infrared", in proceedings of SPIE 8433, Laser Sources and Applications, Photonics Europe 2012, Brussels, Belgium, 2012. DOI: 10.1117/12.915718
19. Sabatini, R., Richardson, M. A., Cantiello, M., Toscano, M., and Fiorini, P., "A novel approach to night vision imaging systems development, integration and verification in military aircraft", Aerospace Science and Technology, 2013. DOI: 10.1016/j.ast.2013.08.021
20. Gardi, A., Sabatini, R., Ramasamy, S., and Kistan, T., "Real-Time Trajectory Optimisation Models for Next Generation Air Traffic Management Systems", Applied Mechanics and Materials, vol. 629, pp. 327-332, 2014. DOI: 10.4028/www.scientific.net/AMM.629.327
21. Gardi, A., Sabatini, R., Ramasamy, S., and de Ridder, K., "4-Dimensional Trajectory Negotiation and Validation System for the Next Generation Air Traffic Management", in proceedings of AIAA Guidance, Navigation, and Control Conference 2013 (GNC 2013), Boston, MA, USA, 2013. DOI: 10.2514/6.2013-4893